Appl Phys B (2010) 101: 119–127
DOI 10.1007/s00340-010-4001-2

Applied Physics B
Lasers and Optics

High-gain Al_2O_3:Nd^{3+} channel waveguide amplifiers at 880 nm, 1060 nm, and 1330 nm

J. Yang · K. van Dalfsen · K. Wörhoff · F. Ay · M. Pollnau

Received: 2 February 2010 / Published online: 14 July 2010

Abstract Neodymium-doped aluminum oxide films with a range of Nd^{3+} concentrations are deposited on silicon wafers by reactive co-sputtering, and single-mode channel waveguides with various lengths are fabricated by reactive ion etching. Photoluminescence at 880, 1060, and 1330 nm from the Nd^{3+} ions with a lifetime of 325 µs is observed. Internal net gain at 845–945 nm, 1064, and 1330 nm is experimentally and theoretically investigated under continuous-wave excitation at 802 nm. Net optical gain of 6.3 dB/cm at 1064 nm and 1.93 dB/cm at 1330 nm is obtained in a 1.4-cm-long waveguide with a Nd^{3+} concentration of 1.68×10^{20} cm^{-3} when launching 45 mW of pump power. In longer waveguides a maximum gain of 14.4 dB and 5.1 dB is obtained at these wavelengths, respectively. Net optical gain is also observed in the range 865–930 nm and a peak gain of 1.57 dB/cm in a short and 3.0 dB in a 4.1-cm-long waveguide is obtained at 880 nm with a Nd^{3+} concentration of 0.65×10^{20} cm^{-3}. By use of a rate-equation model, the gain on these three transitions is calculated, and the macroscopic parameter of energy-transfer upconversion as a function of Nd^{3+} concentration is derived. The high internal net gain indicates that Al_2O_3:Nd^{3+} channel waveguide amplifiers are suitable for providing gain in many integrated optical devices.

J. Yang (✉) · K. van Dalfsen · K. Wörhoff · F. Ay · M. Pollnau
Integrated Optical Micro Systems Group, MESA+ Institute for Nanotechnology, University of Twente, P.O. Box 217, 7500 AE Enschede, The Netherlands
e-mail: j.yang@ewi.utwente.nl
Fax: +31-53-489-3343

1 Introduction

Over the last two decades there has been significant interest in rare-earth-ion-doped planar waveguide amplifiers [1–9] for integrated optical applications. Such low-cost, compact components can be very useful for amplifying optical signals at a high data rate of 170 Gbit/s [8] and compensating optical losses owing to waveguide materials, signal routing, and input/output coupling within an integrated optical circuit.

Neodymium-doped waveguide amplifiers [1–3, 5, 6] and lasers [10–12] are of interest for applications at the ion's specific emission wavelengths. The Nd^{3+}1060-nm gain transition ($^4F_{3/2} \rightarrow {}^4I_{11/2}$) has been widely studied. It has a four-level-energy structure and a large emission cross-section, which provides significant gain at low excitation power for optical amplification. Emission on the $^4F_{3/2} \rightarrow {}^4I_{9/2}$ ground-state transition around 865–930 nm is of interest for signal amplification in integrated optical applications, e.g., data transmission in optical interconnects [13–16] and medical diagnostics [17, 18]. Furthermore, the excited-state transition $^4F_{3/2} \rightarrow {}^4I_{13/2}$ at 1330 nm, corresponding to the wavelength of the second standard telecommunication window, is used for high-speed amplification of optical signals at the telecommunication O-band (1260–1360 nm).

Amorphous aluminium oxide (a-Al_2O_3) has been investigated as a gain material due to its low loss, good mechanical stability and—compared to other amorphous dielectric materials—large thermal conductivity and refractive index, the latter property allowing high integration density [7]. Besides, Al_2O_3 is compatible with Si-based technology. Previously, Er-doped Al_2O_3 has been studied as a gain medium and a peak gain of 2 dB/cm at 1533 nm, and net gain over a wide wavelength range of 80 nm has been demonstrated [9].

In this work, Al_2O_3 is used as the host material for Nd^{3+}. A maximum 14.4-dB and 5.1-dB gain is demonstrated

at 1064 nm and 1330 nm, respectively, in a 4.1-cm-long Al_2O_3:Nd^{3+} channel waveguide. In addition, gain around 865–930 nm is observed, and a peak gain of 3.0 dB at 880 nm is achieved. Energy-transfer upconversion (ETU) of Nd^{3+} ions in the Al_2O_3 host is studied by measuring luminescence decay curves, as well as in gain calculations by use of a rate-equation model. The macroscopic ETU parameter as a function of Nd^{3+} concentration is derived.

2 Waveguide fabrication and spectroscopic characterization

2.1 Waveguide fabrication

Deposition of planar Al_2O_3 waveguides with and without rare-earth-ion dopants has been optimized by use of an AJA ATC 1500 reactive sputtering system equipped with RF sputtering guns, resulting in layers with low background loss [7]. Here, Al_2O_3:Nd^{3+} layers with a thickness of 600 nm were reactively co-sputtered by the same system onto 8-μm thermally oxidized Si wafers. High-purity Al and Nd metallic targets were sputtered using Ar guns, while oxygen was supplied as a gas. By varying the Nd-target power, layers have been obtained with seven different Nd^{3+} concentrations of 0.65, 0.90, 1.13, 1.40, 1.68, 2.50, and 2.95×10^{20} cm^{-3}. The spectroscopic characterization and gain study presented in this paper is based mainly on the four concentrations of 0.65, 1.13, 1.68, and 2.95×10^{20} cm^{-3}, while investigations of the other three intermediate concentrations are discussed briefly. The refractive index of these layers was determined with the prism coupling method to be 1.669 at 633 nm.

Straight channel waveguides were fabricated in the layers by standard lithography and reactive ion etching with a BCl_3–HBr plasma [19]. One half of each layer was left unpatterned for planar waveguide experiments. The channels have a width of 2.0 μm and shallow etch depth of ∼70 nm, using air as the cladding. The etch depth, layer thickness, and waveguide width were selected to ensure strong confinement of the propagating optical signal within the uniformly doped Al_2O_3:Nd^{3+} layers and single-mode behavior with excellent overlap of signal and pump modes. The waveguide samples were cleaved to different lengths varying from 0.85 to 4.25 cm.

2.2 Loss measurements

The broadband loss spectra of Al_2O_3:Nd^{3+} layers were measured using the prism coupling method. White light from a broadband source (FemtoPower1060, SC450, Fianium) was coupled into the film and out again after propagating an adjustable distance through the film by use of two

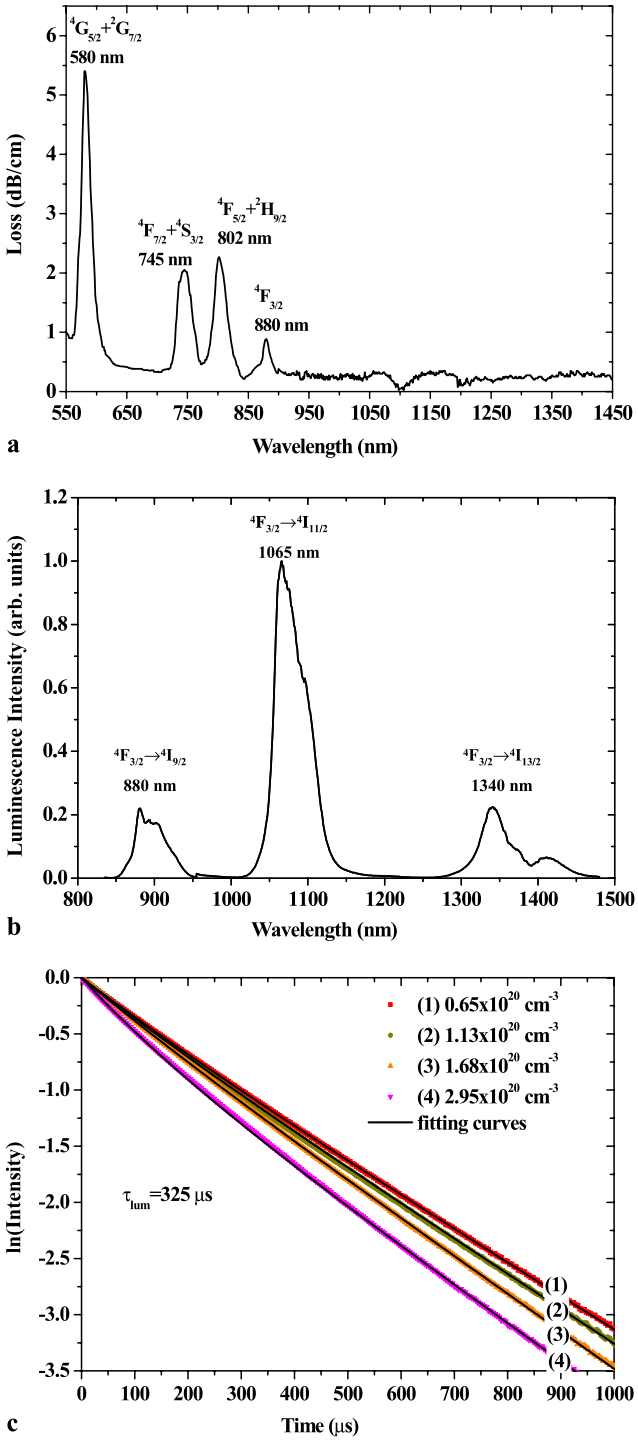

Fig. 1 (**a**) Broadband spectrum of propagation loss and Nd^{3+} absorption in an Al_2O_3:Nd^{3+} slab waveguide; (**b**) broadband luminescence spectrum (corrected with respect to the response curve of the detector) of an Al_2O_3:Nd^{3+} channel waveguide; (**c**) measured (*dots*) and fitted (*line*) luminescence decay curves at 1065 nm for four different Nd^{3+} concentrations (for clarity of the figure, the intermediate three concentrations are not shown here) in Al_2O_3:Nd^{3+} channel waveguides

Table 1 Radiative decay rates $A_{JJ'}$, radiative lifetime τ_{rad}, and branching ratios B of Al_2O_3:Nd^{3+} predicted by Judd–Ofelt analysis

Transition	Wavelength (nm)	$A_{JJ'}$ (s^{-1})	τ_{rad} (μs)	B
$^4F_{3/2} \rightarrow {}^4I_{9/2}$	~880	676.1	474	0.3206
$^4F_{3/2} \rightarrow {}^4I_{11/2}$	~1060	1164.7	474	0.5522
$^4F_{3/2} \rightarrow {}^4I_{13/2}$	~1330	255.1	474	0.1210
$^4F_{3/2} \rightarrow {}^4I_{15/2}$	~1800	13.1	474	0.0062

prisms. The transmission spectra were collected by a large-core liquid fiber and recorded by a spectrometer (Jobin Yvon iHR550). The loss spectrum of the film (Fig. 1a) was derived by a least squares fitting of the recorded spectra. The absorption peaks at 580, 745, 800, and 880 nm are due to absorption transitions from the $^4I_{9/2}$ ground state into the $^4G_{5/2} + {}^2G_{7/2}$, $^4F_{7/2} + {}^4S_{3/2}$, $^4F_{5/2} + {}^2H_{9/2}$, and $^4F_{3/2}$ excited states of Nd^{3+}, respectively.

The loss in Al_2O_3 channel waveguides has been investigated in previous work [7, 19], which indicated that very low extra propagation losses were introduced in channel waveguides by patterning. In this work, the propagation losses in channel waveguides at each wavelength were determined by detecting luminescence or scattered signal light along the propagation direction by use of a CCD camera and software analysis [20, 21]. Additional channel propagation losses of 0.6, 0.3, and 0.15 dB/cm were measured in Al_2O_3:Nd^{3+} channel waveguides at 880, 1064, and 1330 nm, respectively.

The Judd–Ofelt theory [22, 23] for the investigation of $4f$ transitions in rare-earth-ion-doped materials was applied for studying the optical transitions of Nd^{3+} in Al_2O_3. The Judd–Ofelt parameters of Nd^{3+} were determined with the aid of the Nd^{3+} absorption bands measured in our waveguides, which were obtained by subtracting the background propagation loss in Fig. 1a. The obtained values are $\Omega_2 = 5.73 \times 10^{-20}$ cm^2, $\Omega_4 = 2.43 \times 10^{-20}$ cm^2, $\Omega_6 = 5.19 \times 10^{-20}$ cm^2. With these parameters, the radiative decay rates $A_{JJ'}$, radiative lifetimes τ_{rad}, and branching ratios B were obtained and are presented in Table 1.

2.3 Luminescence measurements

By pumping a channel waveguide at 802 nm with a Ti:Sapphire laser, the luminescence spectrum was measured using a spectrometer (Jobin Yvon iHR550), see Fig. 1b. Three distinct emission bands with peaks at 880, 1065, and 1340 nm were observed, which correspond to Nd^{3+} transitions from the metastable $^4F_{3/2}$ level to the $^4I_{9/2}$, $^4I_{11/2}$, and $^4I_{13/2}$ levels, respectively. Compared to the Nd^{3+} luminescence in crystals, which consists of a number of separate sharp peaks due to transitions between individual crystal-field levels [24], the Nd^{3+} luminescence bands in amorphous Al_2O_3 are broader and much less structured because of inhomogeneous line broadening, thus providing large gain bandwidths in an optical amplifier.

Luminescence decay measurements of Nd^{3+} in Al_2O_3 were performed using an external-cavity diode laser (Tiger, Sacher Lasertechnik) emitting at 802 nm as the excitation source. The laser diode was modulated by an external square-pulse generator and delivered pulses of 4-ms duration, allowing the excitation of the Nd^{3+} system to reach a steady state before the pump was switched off. The luminescent light was collected from the waveguide surface by a large-core liquid fiber. Figure 1c shows the luminescent decay curves measured at 1065 nm for four different Nd^{3+} concentrations. In the decay curve (1) for the lowest concentration, except for a faster decay occurring during the first ~50 μs after switching off the pump excitation, which is attributed to energy-transfer upconversion (ETU) between neighboring Nd^{3+} ions in their $^4F_{3/2}$ excited levels [25, 26], an exponential decay was observed. A luminescence lifetime of 325 μs was derived from the exponential part of the decay curve, which was independent of the excitation intensity. It is of the same order of magnitude as the radiative lifetime of 474 μs calculated by Judd–Ofelt analysis from the data of Table 1. The decay curves (2)–(4) for higher Nd^{3+} concentrations exhibit an increasingly nonexponential decay owing to the effect of ETU. The study of ETU parameters of Nd^{3+} from the measured luminescence decay curves will be discussed in Sect. 4, together with an ETU study including the measured gain and a rate-equation model.

3 Optical gain investigation

3.1 Gain measurement

A pump-probe method was used for the small-signal-gain measurement. Pump light was provided by a Ti:Sapphire laser operating at 802 nm. Diode lasers at 880 and 1330 nm and a Nd:YAG laser at 1064 nm were applied as the signal sources. Alternatively, for investigating the broadband gain spectrum at the $^4F_{3/2} \rightarrow {}^4I_{9/2}$ ground-state transition, the Ti:Sapphire laser was tuned around 845–945 nm and used as the signal source, while an external-cavity diode laser operating at 802 nm was applied as pump source. After attenuation of the signal power to typically 1–10 μW the small-signal gain could be measured. A mechanical chopper was inserted into the signal beam path and connected to a lock-in amplifier. Pump light and modulated signal light were combined by a dichroic mirror and coupled into and out of the waveguide via microscope objectives. The unabsorbed pump light coupled out of the waveguide was blocked by a high-pass filter (RG830 or RG850), while the transmitted signal light was measured by a germanium photodiode and

amplified with the lock-in technique. The optical gain was determined by measuring the ratio of the transmitted signal intensities I_p and I_u in the pumped and unpumped case, respectively. By subtracting the waveguide background propagation and absorption losses $\alpha(\lambda)$ (dB/cm) at the signal wavelength, the internal net gain was obtained by calculating the small-signal-gain coefficient in dB/cm from the equation

$$\gamma_{\text{meas}}(\lambda) = 10 \cdot \log_{10}\big(I_p(\lambda)/I_u(\lambda)\big)/l - \alpha(\lambda), \qquad (1)$$

where l is the length of the waveguide channel. This approach eliminates coupling losses that occur in the measurement from the evaluation and provides the gain experienced by the launched signal power along the waveguide.

3.2 Gain at 880 nm, 1064 nm and 1330 nm

For a four-level gain transition, the gain peak is expected at the peak luminescence wavelength of the transition. The same accounts for a three-level transition at high population inversion, as is typically the case under the chosen pump conditions for the waveguide geometries investigated here. Therefore, the internal net gain in our channel waveguides was measured at 880 nm (Fig. 2a) and 1064 nm (Fig. 2b), corresponding to the luminescence peaks of the $^4F_{3/2} \rightarrow {}^4I_{9/2}$ and $^4F_{3/2} \rightarrow {}^4I_{11/2}$ transitions, respectively. For the transition $^4F_{3/2} \rightarrow {}^4I_{13/2}$, due to the availability of signal source, the gain was measured at 1330 nm (Fig. 2c), at which the emission cross section has a value equaling 75% of its peak value at 1340 nm. For each Nd^{3+} concentration, internal net gain at three to four different waveguide lengths was investigated to simultaneously maximize pump-light absorption and minimize excess propagation losses as well as, at the three-level transition, reabsorption at the signal wavelength.

The results of Fig. 2, which were measured with a launched pump power of 45 mW, show a maximum gain of 14.4 dB at 1064 nm and 5.1 dB at 1330 nm, for a Nd^{3+} concentration of 1.13×10^{20} cm^{-3} and a sample length of 4.1 cm. At 880 nm a peak gain of 3.0 dB was obtained in 3.0− and 4.1-cm-long waveguides with Nd^{3+} concentrations of 1.13×10^{20} cm^{-3} and 0.65×10^{20} cm^{-3}, respectively.

Figure 3a displays the internal net gain per unit length measured for seven different Nd^{3+} concentrations at a short channel length (0.85–1.00 cm for gain at 880 nm and 1.30–1.65 cm for gain at 1064 and 1330 nm). At such short lengths the pump power was not completely absorbed, i.e., it became possible to optimize the Nd^{3+} concentration at the three wavelengths. A maximum gain per unit length of 6.3 dB/cm and 1.93 dB/cm at 1064 nm and 1330 nm, respectively, was observed in samples with a concentration of 1.68×10^{20} cm^{-3}, while a maximum 1.57 dB/cm gain was measured at 880 nm in a sample with 1.40×10^{20} cm^{-3} concentration. Figure 3b shows the gain in dB/cm versus launched pump power in these three samples with optimum Nd^{3+} concentration and channel length. The gain saturation at higher pump power is mainly due to the ETU processes from $^4F_{3/2}$ [25, 26].

As not all the Nd^{3+} ions are excited in long samples due to the limitation of launched pump power and concentration-

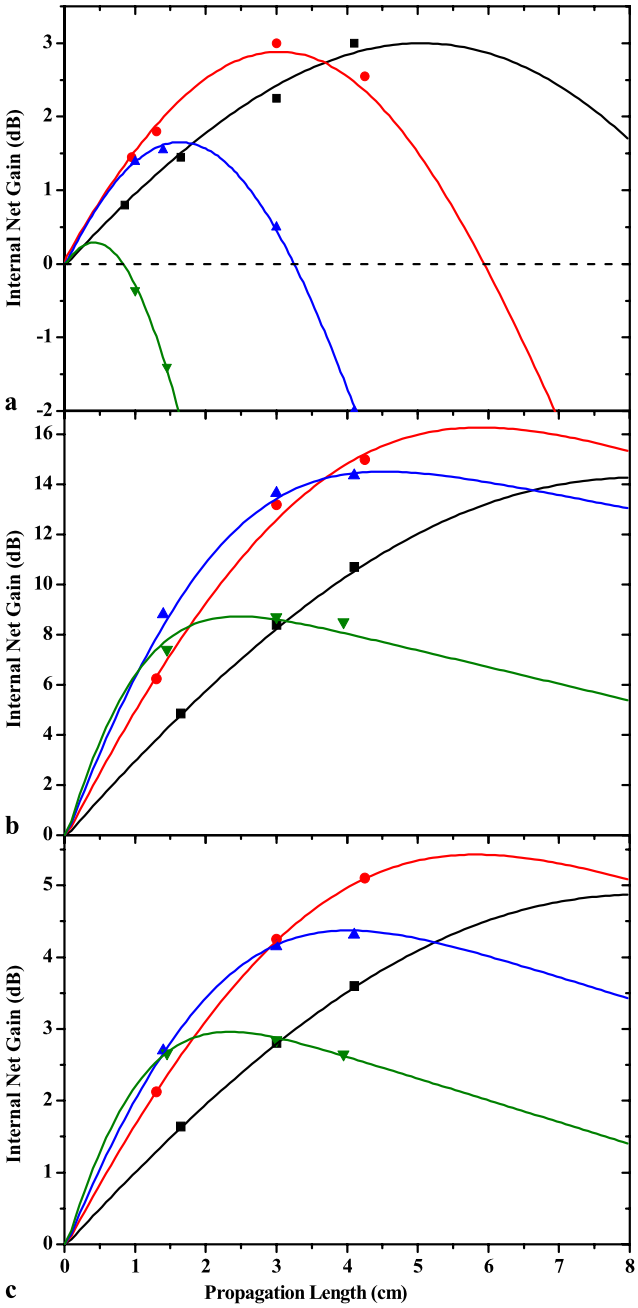

Fig. 2 Measured (*dots*) and calculated (*lines*) internal net gain at (**a**) 880 nm, (**b**) 1064 nm, and (**c**) 1330 nm versus propagation length for a launched pump power of 45 mW with different Nd^{3+} concentrations: 0.65×10^{20} cm^{-3} (■ —), 1.13×10^{20} cm^{-3} (● —), 1.68×10^{20} cm^{-3} (▲ —), 2.95×10^{20} cm^{-3} (▼ —)

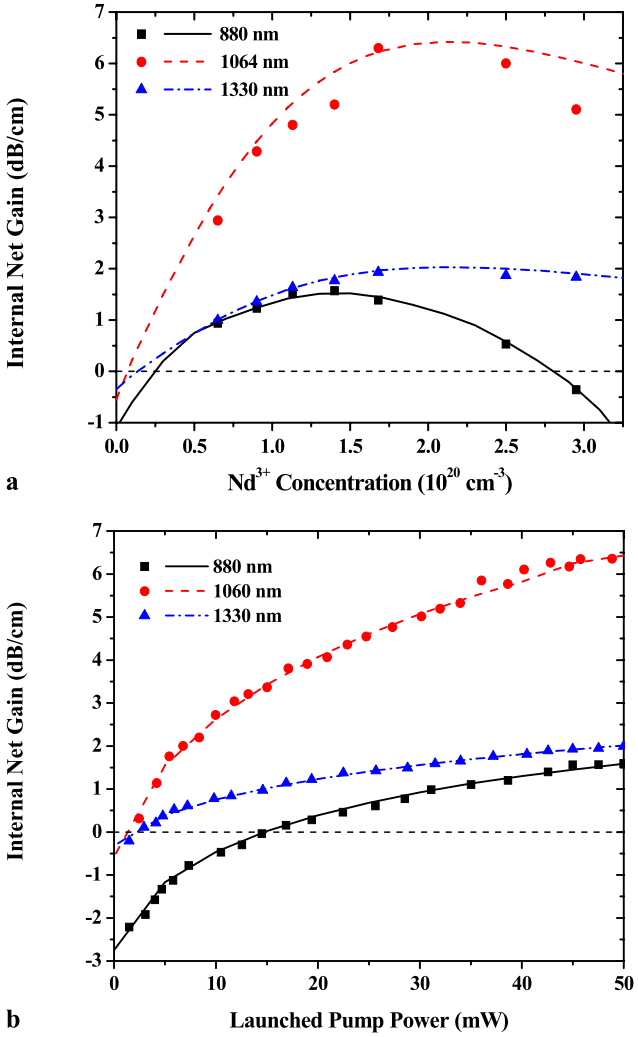

Fig. 3 Measured (*dots*) and calculated (*line*) internal net gain per unit length at 880, 1064, and 1330 nm versus (**a**) Nd^{3+} concentration for a launched pump power of 45 mW and (**b**) launched pump power for the samples with maximum gain per unit length in (**a**)

dependent Nd^{3+} absorption, the gain per unit length decreases for long propagation length. In the heavily Nd^{3+}-doped (2.95×10^{20} cm^{-3}) samples, the 45-mW launched pump power was absorbed completely within the first 2 cm of the channel. Consequently, there was no contribution to gain but only added propagation and potentially absorption loss at longer lengths. Since reabsorption of signal light is negligible at 1064 nm and 1330 nm, higher total gain can be achieved at these two transitions in longer samples with sufficient launched pump power. Therefore, the Nd^{3+} concentration of 1.68×10^{20} cm^{-3}, which provides maximum gain per unit length at 1064 and 1330 nm, is the optimal Nd^{3+} concentration for gain at these two wavelengths in our waveguides. At 880 nm, although gain of 1.57 dB is reached in a 1.0-cm-long sample, the total gain drops significantly when increasing the channel length owing to strong reabsorption of signal light by Nd^{3+} ions in their ground state. The reabsorption of Nd^{3+} must be taken into account when studying the gain at the Nd^{3+} ground-state transition.

3.3 Gain spectrum at 845–945 nm

Since the three-level transition $^4F_{3/2} \rightarrow {}^4I_{9/2}$ exhibits wavelength-dependent reabsorption losses when the inversion is incomplete, the gain spectrum over the whole luminescence bandwidth was investigated. The gain spectrum can be calculated from the absorption and emission cross sections of Nd^{3+} in Al_2O_3 using the equation

$$\sigma^s_{\text{gain}}(\lambda) = \beta \cdot \sigma^s_{\text{em}}(\lambda) - (1-\beta) \cdot \sigma^s_{\text{abs}}(\lambda), \tag{2}$$

where $\sigma^s_{\text{gain}}(\lambda), \sigma^s_{\text{em}}(\lambda)$, and $\sigma^s_{\text{abs}}(\lambda)$ are the wavelength-dependent gain, emission, and absorption cross sections, respectively, at the signal wavelength, and β is the fraction of excited Nd^{3+} ions.

The Nd^{3+} absorption cross section $\sigma^s_{\text{abs}}(\lambda)$ in cm^2 was derived from the equation

$$\sigma^s_{\text{abs}}(\lambda) = \alpha_{\text{Nd}}(\lambda) / \big(10 \cdot \log(e) \cdot N_0 \cdot \Gamma\big), \tag{3}$$

where N_0 is the Nd^{3+} concentration in cm^{-3}, $\alpha_{\text{Nd}}(\lambda)$ is the absorption coefficient as obtained from Fig. 1a by subtracting the background loss, and Γ is the confinement factor in the Al_2O_3:Nd^{3+} layer. The emission cross section $\sigma^s_{\text{em}}(\lambda)$ was determined with the Füchtbauer–Ladenburg equation [27]

$$\sigma^s_{\text{em}}(\lambda) = \frac{\lambda^4 B}{8\pi c n^2 \tau_{\text{rad}}} \frac{I(\lambda)}{\int I(\lambda)\, d\lambda}, \tag{4}$$

where c is the speed of light in vacuum, n is the refractive index of the medium, and $I(\lambda)$ is the intensity of measured luminescent light. The branching ratio B and radiative lifetime τ_{rad} were taken from Table 1. Both spectra are displayed in Fig. 4a. As shown in the figure, the spectra can be converted to each other by use of the McCumber theory [28],

$$\sigma_{\text{em}}(\lambda) = \sigma_{\text{abs}}(\lambda) \cdot \frac{Z_0}{Z_1} \cdot \exp\left(\frac{E_0 - E(\lambda)}{kT}\right), \tag{5}$$

where Z_0/Z_1 is the energy partition function based on the Stark splitting and thermal distribution of the population of the ground and excited states, E_0 is the zero-line energy, $E(\lambda)$is the transition energy for the wavelength λ, k is Boltzmann's constant, and T is the temperature. Equal peak heights and good agreement of the spectral shapes are obtained for a partition function of $Z_0/Z_1 = 2.3$. The peak absorption and emission cross sections in Al_2O_3:Nd^{3+} at 880 nm are 0.35×10^{-20} cm^2 and 0.82×10^{-20} cm^2, respectively.

In order to compare the calculated and measured internal net gain spectra, the internal net gain coefficient in dB/cm

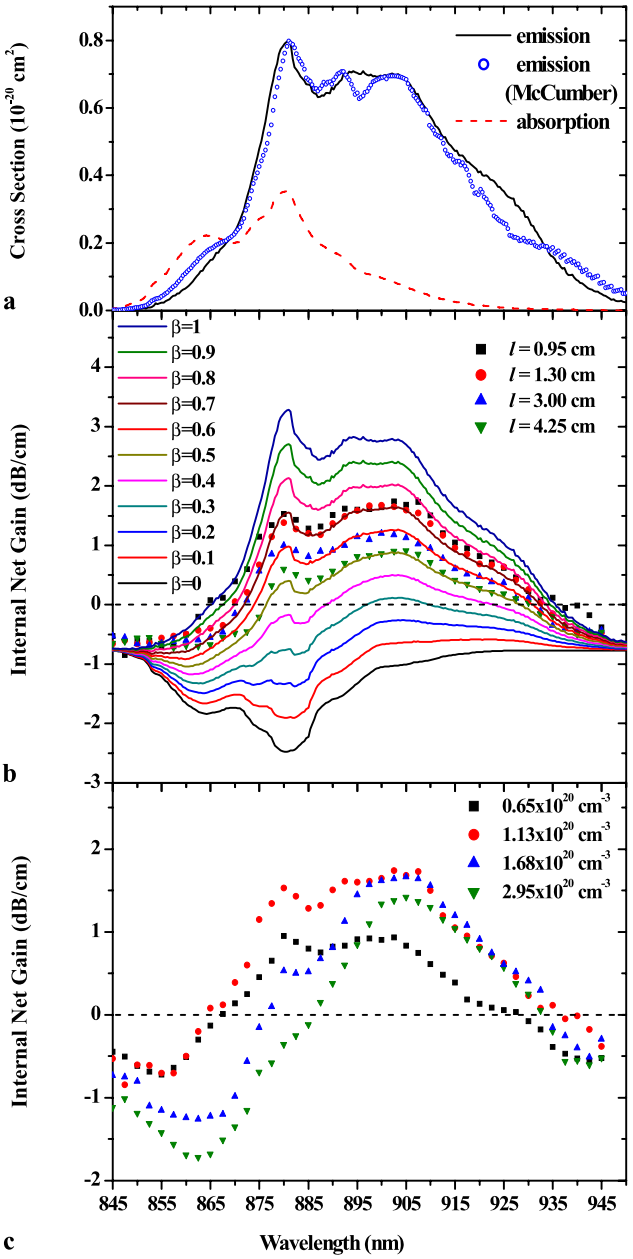

Fig. 4 Spectroscopic measurement at 845–950 nm of the ${}^4F_{3/2} \leftrightarrow {}^4I_{9/2}$ ground-state transition in Al_2O_3:Nd^{3+} channel waveguides. (**a**) Emission (*solid line*) and absorption (*dash line*) cross sections and emission cross section (*dotted line*) derived from the absorption cross section by McCumber theory; internal net gain at a launched pump power of 45 mW (**b**) for different propagation lengths with Nd^{3+} concentration of 1.13×10^{20} cm^{-3} and (**c**) for different Nd^{3+} concentrations with propagation lengths of 0.85–1.00 cm

was calculated from the gain cross section using the equation

$$\gamma_{\text{calc}}(\lambda) = \sigma^s_{\text{gain}} \cdot 10 \cdot \log(e) \cdot N_0. \tag{6}$$

Figure 4b compares the gain spectrum at 845–945 nm calculated for different excitation fractions to those measured in waveguides with four different channel length, for a Nd^{3+} concentration of 1.03×10^{20} cm^{-3} and a launched pump power of 45 mW. The measured and calculated internal net gain spectra show good agreement at excitation fractions β of 0.72, 0.69, 0.62, and 0.54 for sample lengths of 0.95, 1.30, 3.00, and 4.25 cm, respectively. As expected, the results of Fig. 4b show that the gain peak on the ground-state transition is not always at the luminescence peak but strongly depends on population inversion. For high excitation fractions, the gain peak is close to the luminescence peak at 880 nm, while for low excitation fractions, the gain peak moves to longer wavelengths.

The gain spectrum was also measured with channel length of 0.85–1.00 cm for various Nd^{3+} concentrations at a launched pump power of 45 mW (Fig. 4c). From the measured results in Figs. 4b and 4c, the broadest gain bandwidth observed in our waveguides was 865–930 nm.

4 Simulations and ETU parameter

With the aid of a rate-equation model, the optical gain in our waveguides at 880, 1064, and 1330 nm was simulated, and the ETU parameter was determined as a function of Nd^{3+} concentration by fitting the simulated to the experimental results. In addition, the ETU parameter was determined from the measured luminescence decay curves.

4.1 Rate-equation model and gain simulation

The Nd^{3+} transition ${}^4F_{3/2} \rightarrow {}^4I_{9/2}$ around 880 nm is a three-level transition. Nd^{3+} ions are excited at 802 nm from the ground state ${}^4I_{9/2}$ to the pump level ${}^4F_{5/2}$ followed by a fast decay to the metastable excited state ${}^4F_{3/2}$. Since all other excited states in Nd^{3+} exhibit fast multiphonon relaxation and have very short lifetimes, the rate equations describing the population mechanisms of this system can be simplified as follows [25, 26]:

$$dN_4/dt = R_{05} - R_{40} + R_{04} - \tau_4^{-1} N_4 - W_{\text{ETU}} N_4^2, \tag{7}$$

$$N_0 = N_d - N_4, \tag{8}$$

where N_4 and τ_4 are the population density and lifetime of the ${}^4F_{3/2}$ level, respectively, N_0 is the ground-state population density, and N_d is the dopant concentration. To study the effect of ETU, three ETU processes originating in the metastable ${}^4F_{3/2}$ level of the Nd^{3+} system were taken into account and expressed by a single macroscopic parameter W_{ETU} in the simulation, as these processes lead to similar results concerning the population dynamics in the Nd^{3+} system [25]. The rates of pump absorption R_{05}, signal reabsorption R_{04} and stimulated emission R_{40} can be expressed

as follows:

$$R_{05} \approx \sigma_{\text{abs}}^{p} \frac{\lambda_p}{hc} I_p N_0, \tag{9}$$

$$R_{04} \approx \sigma_{\text{abs}}^{s} \frac{\lambda_s}{hc} I_s N_0, \tag{10}$$

$$R_{40} \approx \sigma_{\text{em}}^{s} \frac{\lambda_s}{hc} I_s N_4, \tag{11}$$

where σ_{abs}^{p}, σ_{abs}^{s}, and σ_{em}^{s} are the pump-absorption, signal-absorption, and stimulated-emission cross sections, λ_p and λ_s are the wavelengths and I_p and I_s the intensities of pump and signal light, respectively, launched into the waveguide in propagation direction z, and h is Planck's constant. At steady state, we can solve the above equations analytically.

Since the terminating states $^4I_{11/2}$ and $^4I_{13/2}$ of the transitions at 1064 and 1330 nm, respectively, exhibit a very short lifetime on the order of a few ns, these transitions constitute four-level systems. The reabsorption at the signal wavelength can be neglected, and the rate equations can be simplified further as follows:

$$dN_4/dt = R_{05} - R_{4i} - \tau_4^{-1} N_4 - W_{\text{ETU}} N_4^2, \quad i = 1, 2, \tag{12}$$

$$N_0 = N_d - N_4, \tag{13}$$

$$R_{4i} \approx \sigma_{\text{em}}^{s} \frac{\lambda_s}{hc} I_s N_4, \quad i = 1, 2. \tag{14}$$

In addition to discretization in the propagation direction z, a radial discretization [23, 24] was included in the simulation. The optical mode profiles and confinement of optical power within the polymer channel waveguides were determined by the finite difference method and using geometry and refractive indices of the channel waveguides (Table 2), with the aid of the FieldDesigner software package (PhoeniX [29]). The percentage of pump and signal power outside the active region, which does not contribute to the population dynamics, was not taken into account in the simulation. The optical mode profiles were then approximated by Gaussian profiles. The amount of pump or signal power $P_{P/S}(r, z)$ passing through a circle of radius r at a propagation distance z is described by the equation

$$P_{P/S}(r, z) = P_{P/S,\text{total}}(z)\left[1 - \exp\left(\frac{-2r^2}{w_{P/S}^2}\right)\right], \tag{15}$$

where $P_{P/S,\text{total}}(z)$ is the total power propagating at a distance z, and $w_{P/S}$ is the Gaussian beam waist of pump and signal mode, respectively, which is defined as the radial distance at which the optical intensity drops to $1/e^2$ of its peak value. The total remaining power of pump and signal beams were each redistributed in a Gaussian profile before entering the next longitudinal propagation step.

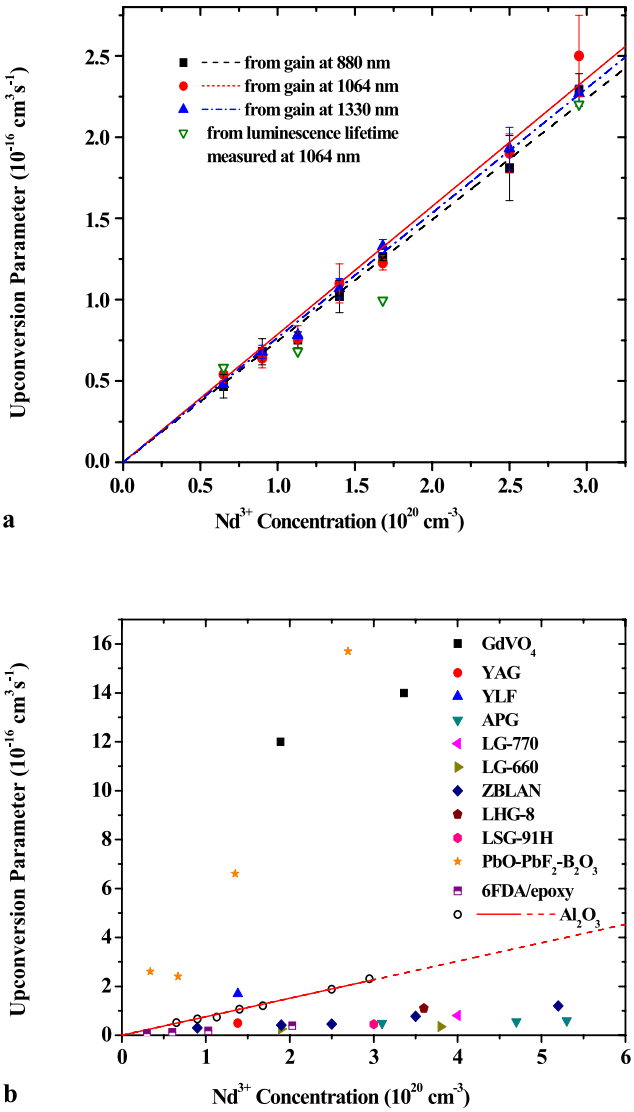

Fig. 5 ETU parameter as a function of Nd^{3+} concentration (**a**) fitted by the rate-equation model at 880, 1064, and 1330 nm and derived from luminescence lifetime measurement at 1064 nm in Al_2O_3:Nd^{3+} and (**b**) taken from the literature for different host materials [6, 25, 26, 30–34]

The experimentally determined spectroscopic parameters (Table 2) were used in the simulation. The population and propagation equations were solved using 128 longitudinal and 32 radial elements. The unknown ETU parameter W_{ETU} was used as the only fit parameter in the simulation. The calculated gain (solid lines) is given together with the measured results in Figs. 2 and 3. The experimental and simulated results are in good agreement with each other.

4.2 ETU parameter

From the simulation of our Al_2O_3:Nd^{3+} channel waveguide amplifiers, the ETU parameter was determined for seven different Nd^{3+} concentrations independently at each of the

Table 2 Simulation parameters of Al_2O_3:Nd^{3+} channel waveguide amplifiers

Parameter	Value			
Nd^{3+} concentration [10^{20} cm^{-3}]	0.65–2.95			
$^4F_{3/2}$ lifetime τ_4 [μs]	325			
Upconversion parameter W_{ETU}	free			
Waveguide thickness [μm]	2.0			
width [μm]	0.6			
Parameter	802 nm	880 nm	1064 nm	1330 nm
Refractive index				
n_{core} (Al_2O_3)	1.660	1.659	1.658	1.649
$n_{lower\text{-}cladding}$ (SiO_2)	1.455	1.454	1.453	1.448
$n_{cladding}$ (air)	1	1	1	1
Waveguide confinement factor	0.91	0.89	0.84	0.75
Gaussian beam waist [μm]				
horizontal w_x	1.48	1.55	1.76	2.17
vertical w_y	0.35	0.37	0.42	0.52
Pump power P_p [mW]	0–50			
intensity I_p [10^{10} W/m^2]	0–4.08			
Signal power P_s [μW]		1	1	1
intensity I_s [10^5 W/m^2]		8.10	7.79	7.71
Cross section [10^{-20} cm^2]				
pump absorption σ^p_{abs}	0.79			
signal reabsorption σ^s_{abs}		0.35		
signal emission σ^s_{em}		0.82	2.01	0.70

three signal wavelengths (Fig. 5a). For each concentration, the values fitted to the gain measured at the three different wavelengths show less than 10% deviation from each other; only for the Nd^{3+} concentration of 0.65×10^{20} cm^{-3}, a deviation of 14% was observed. The deviation is caused by experimental errors in the spectroscopic measurements and gain investigations. The ETU parameter obtained in this way in our waveguides exhibits a linear dependence on Nd^{3+} concentration, see Fig. 5a.

In addition, the ETU parameter was also studied by the measured luminescence decay curves (Fig. 1c). By setting the pump and signal terms to zero and solving (7) or (12) time-dependently, the Bernoulli equation is derived:

$$N_4(t) = \frac{N_4(t=0)\exp(-t/\tau_4)}{1 + W_{ETU} N_4(t=0)\tau_4[1-\exp(-t/\tau_4)]}. \qquad (16)$$

The intrinsic lifetime τ_4 equals the luminescence lifetime obtained from the exponential decay at very low dopant concentration; it remains constant at all dopant concentrations. The ETU parameter was determined by fitting (16) to the measured luminescence decay curves. The fitted curves show very good agreement with the measured decay curves at 1064 nm (see Fig. 1c), which is an indication that this simplified model, assuming a sea of excitations smeared out over the excitation volume by infinitely fast energy migration within the $^4F_{3/2}$ level, is valid for ETU in the Al_2O_3:Nd^{3+} system. With this method, values of the ETU parameter of 0.58, 0.68, 1.00, and 2.20×10^{-16} cm^3 s^{-1} were determined at Nd^{3+} concentrations of 0.65, 1.13, 1.68, and 2.95×10^{20} cm^{-3}, respectively (open dots in Fig. 5a). The main error in this approach is the deviation of the point were $t = 0$ in the decay curve, due to the power fluctuation of the excitation laser.

The deviation of the ETU parameters determined from the two independent approaches is between 6.5–23% for different Nd^{3+} concentration, which is reasonable considering the errors inherent to both approaches. The agreement obtained between the two independent approaches indicates that the obtained values are reliable.

Assuming that the ETU parameter of Nd^{3+} in Al_2O_3 increases linearly with ion concentration, we averaged the values obtained for each concentration. Figure 5b shows the averaged ETU parameter for seven Nd^{3+} concentrations (open circles) and a linear fit. The ETU parameters at different Nd^{3+} concentrations in various materials [6, 25, 26, 30–34] are also displayed in the same figure for comparison. Al_2O_3:Nd^{3+} exhibits a higher ETU parameter

than the majority of glass, polymer, and crystalline materials.

5 Conclusion

Al_2O_3:Nd^{3+} layers have been deposited on thermally oxidized Si substrates, and single-mode channel waveguides have been fabricated. At the investigated signal wavelengths of 880 nm, 1064 nm, and 1330 nm, small-signal gain of 1.57 dB/cm, 6.30 dB/cm, and 1.93 dB/cm, respectively, has been demonstrated for individually optimized Nd^{3+} concentrations. A maximum gain of 3.0 dB, 14.4 dB, and 5.1 dB, respectively, has been obtained. On the ground-state transition, net optical gain has been demonstrated across the wavelength range 865–930 nm, with good agreement between calculated and measured gain spectra. With the gain simulated by a rate-equation model and by fitting of measured luminescence decay curves, the ETU parameter of Nd^{3+} in Al_2O_3 has been studied.

Such waveguide devices may be well suited for providing optical gain in integrated optical applications, e.g., lossless data transmission in optical interconnects and telecommunication, signal enhancement in integrated Raman spectroscopy or lasers integrated into opto-fluidic chips.

Acknowledgements This work was supported by the Dutch Technology Foundation STW and carried out within the framework of project TOE 6986 "Optical Backplanes."

References

1. E. Lallier, J.P. Pocholle, M. Papuchon, M. De Micheli, M.J. Li, Q. He, D.B. Ostrowsky, C. Grezes-Besset, E. Pelletier, Opt. Lett. **15**, 682 (1990)
2. L.H. Slooff, A. van Blaaderen, A. Polman, G.A. Hebbink, S.I. Klink, F.C.J.M. Van Veggel, D.N. Reinhoudt, J.W. Hofstraat, J. Appl. Phys. **91**, 3955 (2002)
3. F. Gardillou, L. Bastard, J.E. Broquin, Appl. Phys. Lett. **85**, 5176 (2004)
4. A. Kahn, H. Kühn, S. Heinrich, K. Petermann, J.D.B. Bradley, K. Wörhoff, M. Pollnau, Y. Kuzminykh, G. Huber, J. Opt. Soc. Am. B **25**, 2008 (1850)
5. J. Yang, M.B.J. Diemeer, D. Geskus, G. Sengo, M. Pollnau, A. Driessen, Opt. Lett. **34**, 473 (2009)
6. J. Yang, M.B.J. Diemeer, G. Sengo, M. Pollnau, A. Driessen, IEEE J. Quantum Electron. **46**, 1043 (2010)
7. K. Wörhoff, J.D.B. Bradley, F. Ay, D. Geskus, T.P. Blauwendraat, M. Pollnau, IEEE J. Quantum Electron. **45**, 454 (2009)
8. J.D.B. Bradley, M. Costa e Silva, M. Gay, L. Bramerie, A. Driessen, K. Wörhoff, J.C. Simon, M. Pollnau, Opt. Express **17**, 22201 (2009)
9. J.D.B. Bradley, L. Agazzi, D. Geskus, F. Ay, K. Wörhoff, M. Pollnau, J. Opt. Soc. Am. B **27**, 187 (2010)
10. D.S. Gill, A.A. Anderson, R.W. Eason, T.J. Warburton, D.P. Shepherd, Appl. Phys. Lett. **69**, 10 (1996)
11. J.R. Lee, H.J. Baker, G.J. Friel, G.J. Hilton, D.R. Hall, Opt. Lett. **27**, 524 (2002)
12. J. Yang, M.B.J. Diemeer, C. Grivas, G. Sengo, A. Driessen, M. Pollnau, Laser Phys. Lett. (2010). doi:10.1002/lapl.201010048
13. S. Uhlig, M. Robertsson, J. Lightw. Technol. **24**, 1710 (2006)
14. J. Moisel, J. Guttmann, H.P. Huber, O. Krumpholz, M. Rode, Opt. Eng. **39**, 673 (2000)
15. S. Lehmacher, A. Neyer, Electron. Lett. **36**, 1052 (2000)
16. L. Dellmann, C. Berger, R. Beyeler, R. Dangel, M. Gmür, R. Hamelin, F. Horst, T. Lamprecht, N. Meier, T. Morf, S. Oggioni, M. Spreafico, R. Stevens, B.J. Offrein, 120 Gb/s optical card-to-card interconnect link demonstrator with embedded waveguides. in *57th Electronic Components and Technology Conference Proceeding* (Reno, 2007), pp. 1288–1293
17. P.J. Caspers, G.W. Lucassen, E.A. Carter, H.A. Bruining, G.J. Puppels, J. Invest. Dermatol. **116**, 434 (2001)
18. P.J. Caspers, G.W. Lucassen, G.J. Puppels, Biophys. J. **85**, 572 (2003)
19. J.D.B. Bradley, F. Ay, K. Wörhoff, M. Pollnau, Appl. Phys. B **89**, 311 (2007)
20. Y. Okamura, S. Yoshinaka, S. Yamamoto, Appl. Opt. **22**, 3892 (1983)
21. A. Kahn, Y. Kuzminykh, H. Scheife, G. Huber, J. Opt. Soc. Am. B **24**, 1571 (2007)
22. B.R. Judd, Phys. Rev. **127**, 750 (1962)
23. G.S. Ofelt, J. Chem. Phys. **37**, 511 (1962)
24. A.A. Kaminskij, *Laser Crystals* (Springer, Berlin, 1979)
25. M. Pollnau, P.J. Hardman, W.A. Clarkson, D.C. Hanna, Opt. Commun. **147**, 203 (1998)
26. M. Pollnau, P.J. Hardman, M.A. Kern, W.A. Clarkson, D.C. Hanna, Phys. Rev. B **58**, 16076 (1998)
27. W.B. Fowler, D.L. Dexter, Phys. Rev. **128**, 2154 (1962)
28. D.E. McCumber, Phys. Rev. A **136**, 954 (1964)
29. PhoenixX. http://www.phoenixbv.com
30. V. Ostroumov, T. Jensen, J.P. Meyn, G. Huber, J. Opt. Soc. Am. B **15**, 1052 (1998)
31. S.A. Payne, G.D. Wilke, L.K. Smith, W.F. Krupke, Opt. Commun. **111**, 263 (1994)
32. J.L. Doualan, C. Maunier, D. Descamps, J. Landais, R. Moncorgé, Phys. Rev. B **62**, 4459 (2000)
33. L.C. Courrol, B.L.S. de Lima, L.R.P. Kassab, V.D. Del Cacho, S.H. Tatumi, L. Gomes, N.U. Wetter, J. Non-Cryst. Solids **348**, 98 (2004)
34. S.L. Oliveira, D.F. de Sousa, A.A. Andrade, L.A.O. Nunes, T. Catunda, J. Appl. Phys. **103**, 023103 (2008)